Effects of quantum-mechanical symmetry on electronic correlations in intrashell states of four-valence-electron atoms

Bao Chengguang

China Center of Advanced Science and Technology (World Laboratory), P. O. Box 8730, Beijing, 100080, People's Republic of China and Department of Physics, Zhongshan University, Guangzbou, 510275, People's Republic of China

(Received 10 January 1994)

A model with all the degrees of freedom of the core and all the radial degrees of freedom of the valence electrons frozen is used to investigate the effects of quantum-mechanical symmetry on electronic correlations of intrashell states of four-valence-electron atoms. A number of different correlative densities have been calculated. A spin-polarity-dependent analysis has been made. The emphasis is placed on the qualitative aspect. The 12 $N=2$ intrashell states of carbon are selected as the object of study; however, the qualitative features extracted are expected to be quite general. The morphology of each state (including the most probable shape, the most probable orientation, and the preferreed modes of internal motion) has been studied. The effect of quantum-mechanical symmetry was found to be decisive.

PACS number(s): 31.50.+w, 03.65.Ge, 31.20.Tz, 31.20.Di

I. INTRODUCTION

The investigation of electronic correlation is a basic task in atomic physics. This paper is dedicated to the intrashell states of four-valence-electron atoms, where the inherent physics is expected to be very rich. There have been preliminary results on four-electron systems [1–4], but very few on four-valence-electron systems (or quadruply excited states) [5,6]. An important feature, namely the existence of collective correlated internal motions, has been revealed in three-valence-electron systems [7,8] and also in the $L=0$ states of four-valence-electron systems [5,6]. This paper is a generalization of [5,6] to $L\neq 0$ states; the emphasis is placed on the qualitative aspect and the analysis is concentrated to reveal the decisive effect of quantum-mechanical (QM) symmetry imposed on the geometric structures and internal motions. Before developing a method for the precise calculation for quantitative purposes, a qualitative analysis is desirable to provide a clear physical picture to govern further quantitative exploration. This is the motivation of this paper.

The carbon atom is chosen as the direct object of study, where four-valence electrons stay in the $N=2$ shell. Nevertheless, the qualitative features extracted are expected to be held also for other four-valence-electron systems (e.g., silicon or quadruply excited intrashell states in general). Two approximations are adopted.

(i) The degrees of freedom of the core electrons are frozen. Since we consider only the cases where the core is entirely filled, this approximation is reasonable.

(ii) The radial degrees of freedom of the valence electrons are frozen. This is called an r-frozen model, which has already been used in the study of $L=0$ states [5,6]. A discussion of the applicability of this model is referred to in [8].

In fact, as we shall see, the basic features of relevant states are essentially determined by the QM symmetry, but not by the details of dynamics. On the other hand, the constraints imposed by the QM symmetry can be fully taken into account under the approximations adopted. Thus the main features of relevant states will not be spoiled by the approximations.

II. PROCEDURE

The Hamiltonian reads

$$H=\frac{\hbar^2}{2mr_0^2}\sum_{i=1}^{4}\hat{l}_i^2+\sum_{i<j}\frac{e^2}{|\mathbf{r}_{ij}|}\ , \tag{1}$$

where $\hat{l}_i$ is an operator corresponding to l_i, which is the orbital angular momentum of the ith electron (e_i) relative to the center. $\mathbf{r}_{ij}=\mathbf{r}_i-\mathbf{r}_j$, $\mathbf{r}_i$ is the position vector of e_i; $\mathbf{r}_i=r_0\hat{\mathbf{r}}_i$ is assumed, where r_0 is given as 0.62 Å to simulate the $N=2$ shell of carbon [9].

The Hamiltonian is going to be diagonalized in a model space spanned by basis functions as

$$\tilde{\Phi}_i=\mathcal{A}\{[(Y_{l_1}(1)Y_{l_2}(2))_{l_{12}}(Y_{l_3}(3)Y_{l_4}(4))_{l_{34}}]_{LM}\times\chi^{M_s}_{s_1s_2S}(1234)\}\ , \tag{2}$$

where $\chi^{M_S}_{s_1s_2S}$ is the spin part, the spins of e_1 and e_2 are coupled to s_1, e_3 and e_4 are coupled to s_2, and s_1 and s_2 are coupled to S. M and M_S are the z components of L and S, respectively. $\mathcal{A}$ is the antisymmetrizer. It is noted that the $\tilde{\Phi}_i$ do not form a orthonormal set; among them linearly dependent components should be excluded from the model space. Let all the l_i be constrained by $0\le l_i\le l_{\max}$; than the dimension of the model space is determined by $l_{\max}$. In what follows, $l_{\max}=2$ is assigned. From the point of view of the independent-electron model, $l_{\max}$ is simply equal to 1 in the $N=2$ shell. Now, the $l_{\max}$, being given as larger, lies in the fact that e-e repulsion may increase the orbital angular momentum of both electrons. If $l_{\max}$ is given even larger than 2, the qualitative features of relevant states are essentially unaffected.

After the diagonalization, eigenstates ψ_i of different

$^{2S+1}L^{\pi}$ symmetries are obtained. Each of them can be decomposed into two parts:

$$\psi_i = \Psi_i^{\mathrm{I}} + \Psi_i^{\mathrm{II}} , \tag{3}$$

where Ψ_i^{I} contains only those components with all $l_i \leq 1$ and Ψ_i^{II} contains those components with at least one l_i ($i=1$, 2, 3, or 4) >1. It was found that the eigenstates can be sharply divided into two groups. The first group contains 12 states, each of them dominated by the Ψ_i^{I} components. The remaining states are contained in the second group, each dominated by the Ψ_i^{II} component. Evidently, the 12 states of the first group, and only these 12 states, are contained in the $N=2$ intrashell states of carbon.

The energy spectrum and the $^{2S+1}L^{\pi}$ labels of these 12 states are given in Fig. 1, where the subscript i denotes the ith lowest state of a given $^{2S+1}L^{\pi}$. Figure 1 shows that the order of the energy levels does not depend on the choice of r_o. Among these states, the four $L=0$ states have already been discussed in [5,6] and the two $^3P^e$ states in [10]; the remaining six states will be discussed in detail in this paper.

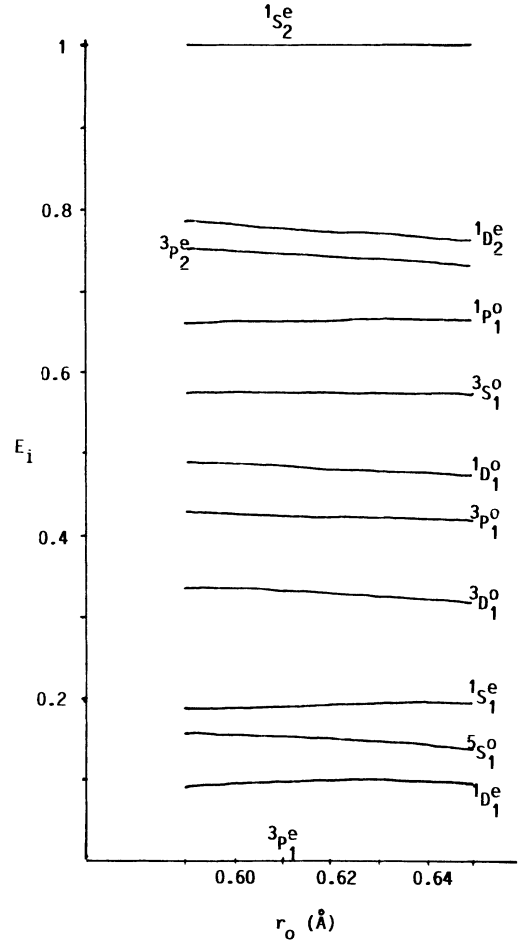

FIG. 1. Energy spectrum of the 12 intrashell states of carbon under the r-frozen approximation. r_0 is given from 0.59 to 0.65 Å. In each case of r_0, the energy of the $^3P_1^e$ ground state is scaled as zero, while the excitation energy of the $^1S_2^e$ (highest) state is scaled as 1. In the cases of $r_0=0.59$, 0.62, and 0.65 Å, the excitation energies of $^1S_2^e$ are 61.9, 56.9, and 52.6 eV, respectively.

Since the correlations are found to be strongly spin-polarity dependent, a polarity-dependent procedure of analysis as in [6,7] is used. The eigenstate is expanded as

$$\psi_i = \sum_{\mu} f^M_{\mu_1\mu_2\mu_3\mu_4}(1234)\xi_{\mu_1}(1)\xi_{\mu_2}(2)\xi_{\mu_3}(3)\xi_{\mu_4}(4) , \tag{4}$$

where $\xi_\mu(i)$ is the spin state of e_i with polarity $\mu=\pm\frac{1}{2}$. $\sum_\mu$ implies a summation over $\mu_1\mu_2\mu_3\mu_4$ fulfilling $\sum_i \mu_i = M_s$. Owing to the antisymmetrization, we have

$$f^M_{\mu_1\mu_2\mu_3\mu_4}(1234) = (-1)^p f^M_{\mu_{p_1}\mu_{p_2}\mu_{p_3}\mu_{p_4}}(p_1p_2p_3p_4) , \tag{5}$$

where $p_1p_2p_3p_4$ is a permutation of 1234 and $(-1)^p$ is the permutation parity. Equation (5) implies that different $f^M_{\mu_1\mu_2\mu_3\mu_4}$ components would provide equivalent information; thus the analysis of only one component is sufficient. In what follows, $M_S=0$ is assumed and mostly the $f^M_{\frac{1}{2}\frac{1}{2}\frac{\bar{1}}{2}\frac{\bar{1}}{2}}$ is selected for analysis; in this choice, e_1 and e_2 have their spins up and e_3 and e_4 have their spins down. Besides, $M=L$ is further assumed; in this choice, we have L essentially lying along the Z axis, thus any anisotropism discussed later is in fact relative to the direction of L.

Since $M_S=0$ has been chosen, additionally we have

$$f^M_{\frac{1}{2}\frac{1}{2}\frac{\bar{1}}{2}\frac{\bar{1}}{2}}(1234) = (-1)^S f^M_{\frac{1}{2}\frac{1}{2}\frac{\bar{1}}{2}\frac{\bar{1}}{2}}(3412) . \tag{6}$$

Equation (6) will facilitate the following analysis. However, before going into the details, let us first inspect the effect of QM symmetry.

III. SYMMETRY

It has been stated in [5] that inherent nodal surfaces (INS) arising from QM symmetry appear in the multidimensional coordinate space at exactly the same locations for all the wave functions of a given $^{2S+1}L^{\pi}$ symmetry. They embody the constraints imposed by the QM symmetry on microscopic states. All the geometric configurations located exactly in the INS are strictly prohibited. Furthermore, if a wave function is distributed closely by the two sides of an INS, the latter will induce a motion normal to the surface and the system will evolve back and forth, crossing the nodal surface repeatedly; thus a nodal surface is associated with a specific mode of motion. Evidently, an INS causes instability; thus, wave functions of lower states are not preferentially distributed close to any INS.

On the other hand, a wave function of lower states would in general preferentially be distributed around a configuration with better geometric symmetry to reduce the potential energy. At the same time, this configuration, as the most probable shape, should be sufficiently far away from any INS to reduce the kinetic energy. With these principles in mind, in what follows a procedure of analysis will be carried out and presumed structures of relevant states will be suggested.

Hereafter, let e_1 and e_2 be the up electrons and e_3 and

e_4 be the down electrons. Let O be the center of mass of e_1 and e_2 and O' be that of e_3 and e_4. When the four-valence electrons stay on a shell, evidently the most favorable configuration is an equilateral tetrahedron (ETH). This configuration should be the first candidate to be pursued. In this shape, we have $r_{12}=r_{34}=\sqrt{2}OO'$ and $\mathbf{r}_{12}\perp\mathbf{r}_{34}\perp\overline{OO'}$. When the ETH has its $\overline{OO'}$ lying in the X-Y plane, it is called a lying ETH; when $\overline{OO'}$ is parallel to the Z axis, it is called a standing ETH. When OO' becomes longer (shorter) than $r_{12}/\sqrt{2}=r_{34}/\sqrt{2}$, it is called a prolonged (flattened) ETH. The following discussion on ETH holds mostly for a prolonged (flattened) ETH.

With a lying ETH, there are essentially three choices of $\mathbf{r}_{12}$: (i) $\mathbf{r}_{12}$ is parallel to the Z axis while $\mathbf{r}_{34}$ is lying in the X-Y plane [Fig. 2(a)]; (ii) $\mathbf{r}_{12}$ is normal to the Z axis while $\mathbf{r}_{34}$ is parallel to the Z axis [Fig. 2(b)]; and (iii) $\mathbf{r}_{12}(\mathbf{r}_{34})$ is neither parallel nor normal to the Z axis. In the first choice, the configuration is invariant under the combined operation $\mathcal{P}R^{Z}_{180}P_{12}$, where $\mathcal{P}$ is a space inversion, R^{Z}_{180} is a rotation about the Z axis by 180°, and P_{12} is an interchange of $\mathbf{r}_1$ and $\mathbf{r}_2$. In the case of $\Pi(-1)^L=+1$ states, the eigenvalue of this combined operator is -1. Thus the wavefunction has to be zero at this configuration; accordingly an INS appears. In the second choice, the configuration is invariant under $\mathcal{P}R^{Z}_{180}P_{34}$; similarly, another INS appears in the $\Pi(-1)^L=+1$ states. In the third choice, a typical case is shown in Fig. 2(c), where $\mathbf{r}_{12}$ ($\mathbf{r}_{34}$) makes a 45° (or 135°) angle with the Z axis. In this case, e_1 is directly opposite e_3 and e_2 is directly opposite e_4 with respect to the Z axis. Hence, the corresponding ETH configuration is invariant under the combined operation $R^{Z}_{180}P_{13}P_{24}$. According to Eq. (6) an INS appears in the $(-1)^{L+S}=-1$ states.

From the above analysis, both the $\Pi(-1)^L=+1$ and the $(-1)^{L+S}=-1$ states would avoid the lying ETH; otherwise, they would be seriously affected by the INS. Hence, among the eight $L\neq 0$ states, the candidates for the lying ETH would be the ${}^3p^e$ and ${}^1D^o$ states. In fact, the most probable shape of the ${}^3p^e_1$ state is indeed a lying ETH as revealed in [10].

When the ETH is standing, the configuration is invariant under $R^{Z}_{180}P_{12}P_{34}$; thus an INS appears in all the $L=$odd states. Besides, this configuration is also invariant under $\mathcal{P}R^{Z}_{90}P_{12}P_{13}P_{24}$; thus an INS appears also in all the $L=$even states with $\Pi(-1)^{L/2+S}=-1$. Hence, among the eight $L\neq 0$ states, the candidates for the standing ETH would be the ${}^1D^e$ and ${}^3D^o$ states.

Due to the existence of the above-mentioned INS, the ${}^1p^o$ and ${}^3p^o$ would not prefer the ETH configuration, but, instead, the coplanar configuration (i.e., the four electrons and the core essentially lying in a plane) may be pursued. In the case of a coplanar rectangle (including the square as a special case), there are two choices: a pair of spin-parallel electrons are put at either adjacent or at opposite vertexes. However, the first choice is prohibited in all $\Pi(-1)^s=-1$ states while the second choice is prohibited in all odd-parity states, simply because a space inversion of the coplanar rectangle is equivalent to an interchange of the particles at the two ends of a diagonal together with an interchange of the other two [refer to Eq. (6)]. Consequently, the ${}^3P^o$ state may pursue a coplanar rectangle with the spin-parallel electrons at adjacent vertexes. In the case of the ${}^1P^o$ state, since two possible choices are both prohibited, it cannot have the coplanar rectangle configuration. Since an ETH [or even a prolonged (flattened) ETH] is also unfavorable in a ${}^1P^o$ state, this state cannot have a configuration with good geometric symmetry; instead, a trapezoid or a noncoplanar rectangle may be favored by this state. The above suggestions will be checked as follows.

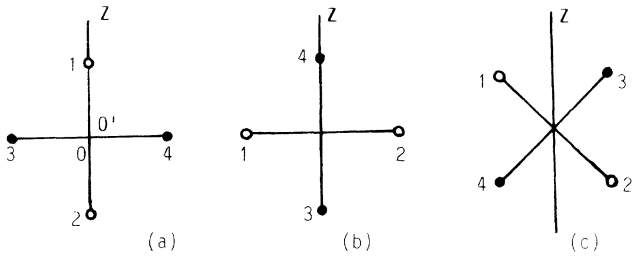

FIG. 2. Three typical orientations of a lying ETH. The Z axis of the fixed frame is chosen to be lying along L. $\overline{OO'}$ is normal to the Z axis and O overlaps O' in each figure. The electrons above the plane are labeled by an open circle and those under the plane by a closed circle.

IV. ${}^1D^e$ STATES

Let us define a body frame Σ' with its $\mathbf{k}'$ axis parallel to $\mathbf{r}_1+\mathbf{r}_2$ and its $\mathbf{i}'$ axis parallel to $\mathbf{r}_2-\mathbf{r}_1$. Let $\alpha'\beta'\gamma'$ denote the Euler angles specifying the Σ' frame. Let θ_{12} be the angle between $\mathbf{r}_1$ and $\mathbf{r}_2$. Then the coordinates of e_1 to e_4 observed in Σ' are $(\theta_{12}/2,\ 180°)$, $(\theta_{12}/2, 0°)$, (θ'_3,ϕ'_3), and (θ'_4,ϕ'_4), respectively; they are also labeled in short by $\hat{\mathbf{r}}'_1$, $\hat{\mathbf{r}}'_2$, $\hat{\mathbf{r}}'_3$ and $\hat{\mathbf{r}}'_4$. With this new set of arguments, the wave function can be expanded as

$$f^L_\mu(1234)=\sum_K D^L_{KL}(-\mathcal{R}')f^K_\mu(\hat{\mathbf{r}}'_1\hat{\mathbf{r}}'_2\hat{\mathbf{r}}'_3\hat{\mathbf{r}}'_4)\ , \tag{7}$$

where μ denotes $(\mu_1\mu_2\mu_3\mu_4)$, $\mathcal{R}'$ denotes the Euler rotation from the fixed frame to the Σ' frame, and K is the component of L along the $\mathbf{k}'$ axis. Then the condition of orthonormality can be written as

$$1=\sum_{\mu_1\mu_2}\int \sin\beta' d\beta' d\gamma' \rho^{\mu_1\mu_2}_{\text{ori}}\ , \tag{8}$$

where

$$\rho^{\mu_1\mu_2}_{\text{ori}}=2\pi\sum_{KK'}D^L_{KL}(-\mathcal{R}')D^{L*}_{K'L}(-\mathcal{R}')\int \sin\theta_{12}d\theta_{12}d\hat{\mathbf{r}}'_3 d\hat{\mathbf{r}}'_4\sum_{\mu_3\mu_4} f^K_\mu f^{K'*}_\mu \delta_{\mu_1+\mu_2+\mu_3+\mu_4,M_S} \tag{9}$$

is the orientation-distribution function of the Σ' frame. This function depends only on β' and γ', but not on α'. $\rho_{\text{ori}}^{\frac{1}{2}\frac{1}{2}}$ of the $^1D_1^e$ and $^1D_2^e$ states are shown in Figs. 3(a) and 3(b).

Let the condition of orthonormality be rewritten as

$$1=\int \sin\theta_{12} d\theta_{12} \rho_2(\theta_{12}) , \tag{10}$$

where

$$\rho_2=\rho_{\uparrow\uparrow}+\rho_{\uparrow\downarrow} , \tag{11}$$

$$\rho_{\uparrow\uparrow}=\frac{8\pi^2}{2L+1}\sum_{\mu}\delta_{\mu_1\mu_2}\sum_{K}\int d\hat{\mathbf{r}}_3' d\hat{\mathbf{r}}_4' |f_{\mu}^{K}|^2 ,$$

$$\rho_{\uparrow\downarrow}=\frac{8\pi^2}{2L+1}\sum_{\mu}(1-\delta_{\mu_1\mu_2})\sum_{K}\int d\hat{\mathbf{r}}_3' d\hat{\mathbf{r}}_4' |f_{\mu}^{K}|^2 . \tag{12}$$

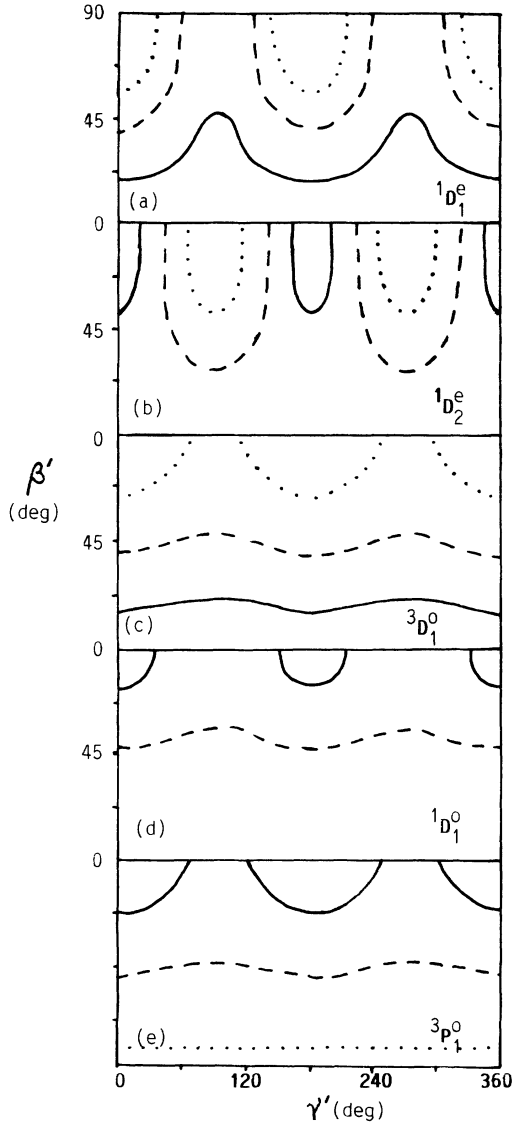

FIG. 3. Orientation-distribution functions $\rho_{\text{ori}}^{\frac{1}{2}\frac{1}{2}}(\beta',\gamma')$. The solid, dashed, and dotted lines give 92%, 64%, and 36% of the maximum, respectively.

$\rho_{\uparrow\uparrow}$ is the spin-parallel two-body density and $\rho_{\uparrow\downarrow}$ is the spin-antiparallel two-body density. The sum of them is just the usual (polarity-blind) two-body density ρ_2. Multiplying $\rho_{\uparrow\uparrow}$, $\rho_{\uparrow\downarrow}$, and ρ_2 by a factor $\sin\theta_{12}$, the weighted two-body densities $\tilde{\rho}_{\uparrow\uparrow}$, $\tilde{\rho}_{\uparrow\downarrow}$, and $\tilde{\rho}_2$ are further defined. $\tilde{\rho}_{\uparrow\uparrow}$ ($\tilde{\rho}_{\uparrow\downarrow}$) gives the probability density of a pair of spin-(anti) parallel electrons with angular separation θ_{12} and with the measurement blind to their orientation and blind to other electrons. These functions are plotted in Figs. 4(a) and 4(b). The optimal value of θ_{12}, where $\tilde{\rho}_{\uparrow\uparrow}$ is peaked, is denoted by $\bar{\theta}_{\uparrow\uparrow}$ and that of the $\tilde{\rho}_{\uparrow\downarrow}$ is denoted by $\bar{\theta}_{\uparrow\downarrow}$; they are given in Table I.

Making use of the above information, further analysis can be restricted in smaller subspaces. Let us define another rotating frame Σ'' with its $\mathbf{k}''$ axis parallel to $\mathbf{r}_3+\mathbf{r}_4$ and its $\mathbf{i}''$ axis parallel to $\mathbf{r}_4-\mathbf{r}_3$. Let $\alpha''\beta''\gamma''$ be another set of Euler angles specifying the Σ'' frame. Let θ_{34} be the angle between $\mathbf{r}_3$ and $\mathbf{r}_4$. Then, $\mathbf{r}_3$ and $\mathbf{r}_4$ can be considered as functions of $\alpha''\beta''\gamma''$ and θ_{34}; similarly, $\mathbf{r}_1$ and $\mathbf{r}_2$ can be considered as functions of $\alpha'\beta'\gamma'$ and θ_{12}. Accordingly, the wave functions can be considered as functions of $\alpha'\beta'\gamma'\alpha''\beta''\gamma''$, θ_{12}, and θ_{34}.

In the case of the $^1D_1^e$ state, let $\alpha'=0$ (this choice is irrelevant); let $\beta'=\gamma'=0°$ [this is associated with an optimal case in Fig. 3(a), and e_1 and e_2 are given in the upper X-Z plane by the two sides of the Z axis as shown in Fig. 5(a)]; and let $\theta_{12}=\theta_{34}=\bar{\theta}_{\uparrow\uparrow}=120°$; then $|f^{L}_{\frac{1}{2}\frac{1}{2}\frac{1}{2}\frac{1}{2}}|^2$ as functions of β'' and γ'' with α'' being specified at a number of values have been observed. A typical case with $\alpha''=0$ is plotted in Fig. 6(a), where the peak occurs at ($\beta''=180°$, $\gamma''=90°$). It implies that e_3 and e_4 prefer to stay in the lower Y-Z by the two sides of the Z axis as shown in Fig. 5(a). Thus, as predicted in Sec. III, this state has the standing ETH as its most probable shape. Incidentally, if α'' is not given at 0, we arrive at exactly the same conclusion.

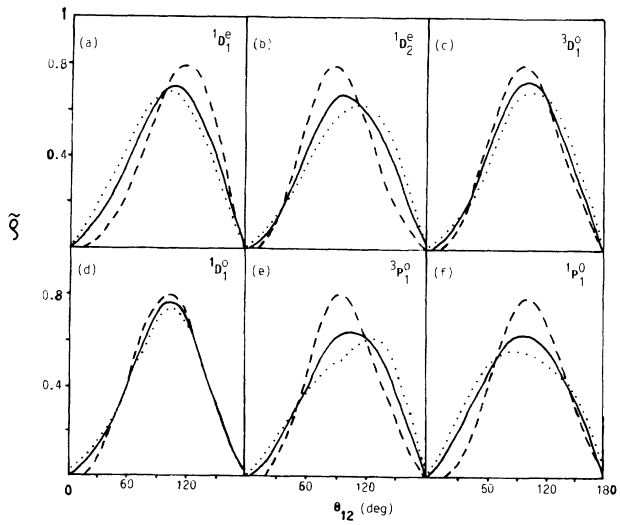

FIG. 4. Weighted two-body densities. The dashed lines gives $\tilde{\rho}_{\uparrow\uparrow}$, the dotted line gives $\tilde{\rho}_{\uparrow\downarrow}/2$, and the solid line gives $\tilde{\rho}_2/3$. The ordinate of each figure is given in arbitrary units.

TABLE I. Most probable angular separations between a pair of spin-parallel electrons ($\bar{\theta}_{\uparrow\uparrow}$) and spin-anti electrons ($\bar{\theta}_{\uparrow\downarrow}$). The values are evaluated under an r-frozen model for the valence electrons of the ($N=2$) intrashell states.

	$^5S_1^o$	$^1S_1^e$	$^3S_1^o$	$^1S_2^e$	$^3P_1^e$	$^3P_1^o$	$^1P_1^o$	$^3P_2^e$	$^1D_1^e$	$^3D_1^o$	$^1D_1^o$	$^1D_2^e$
$\bar{\theta}_{\uparrow\uparrow}$	102°	104°	117°	92°	126°	96°	102°	91°	120°	100°	102°	90°
$\bar{\theta}_{\uparrow\downarrow}$	102°	134°	88°	140°	96°	130°	87°	102°	100°	110°	104°	118°
		85°		66°								

Let us inspect the motion around the most probable shape. We are reminded that, besides the trivial small oscillation around an equilibrium shape, the internal motions are characterized by transformations among different shapes [11]. In our case, there are two particularly important configurations; namely, the ETH and the coplanar square. Accordingly, there are two basic modes relating these two shapes. One is a transformation from an ETH to a coplanar square, and again to an ETH via a variation of OO' (or θ_{12} and θ_{34}) as shown in Fig. 7(a); then this process is repeated but in reverse direction. This was called an ETH-square-ETH (E-S-E) mode [5]. The other one is a similar transformation but via a twist between the two pairs of electrons as shown in Fig. 7(b); this has been called a twist mode [11]. We shall show that both modes in the $^1D_1^e$ state are not energetic.

Starting from a standing ETH with OO' parallel to the Z axis, the E-S-E oscillation would lead to an intermediate structure, which is a coplanar square Lying on the X-Y plane with a pair of spin-parallel electrons at the two ends of each diagonal [as shown at the right of Fig. 7(a)]. This configuration possesses a number of invariances; it is invariant under the combined operation of $\mathcal{P}R^Z_{180}$ [thereby, an INS appears in all $\Pi(-1)^L=-1$ states], under $\mathcal{P}P_{12}P_{34}$ (thereby, an INS appears in all odd-parity states), or under $P_{12}P_{24}P_{13}R^Z_{90}$ [thereby, when $L=$even, an INS appears in all $(-1)^{L/2+S}=+1$ states]. Besides, it is also invariant under a rotation about a diagonal by 180° together with an interchange of the two particles at the other diagonal (thereby, an INS appears in all $L=0$ states). It turns out that among all $N=2$ intrashell states, the $^1D^e$ is the only state which does not contain the above INS; thus it would have a gentle E-S-E oscillation. Similarly, the twist would lead to a standing coplanar square, with the two electrons in the upper (or lower) half of the square being spin parallel. This configuration is also not prohibited by the QM symmetry; thus the $^1D_1^e$ state would not have a very energetic twist motion.

To show the main feature of the wave function, let $\alpha'=\beta'=\gamma'=0°$, $\alpha''=\beta''=0°$, and $\gamma''=90°$ [in this choice, e_1 and e_2 are in the X-Z plane, while e_3 and e_4 are in the Y-Z plane, as shown in Fig. 5(a)]; then the imaginary part of $f^L_{\frac{1}{2}\frac{1}{2}\frac{\bar{1}}{2}\frac{\bar{1}}{2}}$ (meanwhile, the real part is zero) as a function of θ_{12} and θ_{34} is plotted in Fig. 8(a) [when θ_{12} (θ_{34}) $>180°$, the pair of particles are staying under the X-Y plane]. Figure 8(a) shows that the distribution is very smoothly lying along POQ, where the increase of θ_{12} matches the decrease of θ_{34}. P is associated with an ETH, 0 with a square, and Q with, again, an ETH. Thus, the existence of a gentle E-S-E motion is confirmed. During this gentle motion, the probability of being coplanar is quite large, and the whole electronic cloud looks like a flattened ellipsoid perpendicular to L. In fact, the $^1D_1^e$ state is very similar to the $^3P_1^e$ ground state [compare Fig. 8(a) with Fig. 6(a) of [10]]; they both have gentle oscillations around an ETH shape. However, the $^1D_1^e$ has the $\overline{OO'}$ to be most likely parallel to L, while the $^3P_1^e$ has the $\overline{OO'}$ normal to L.

In the case of the $^1D_2^e$ state, let $\alpha'=0°$, $\beta'=90°$, and $\gamma'=0°$ [this is associated with a peak in Fig. 3(b) and e_1 and e_2 are given in the X-Z plane by the two sides of the X axis, as shown in Fig. 5(b)], $\theta_{12}=\theta_{34}=\bar{\theta}_{\uparrow\uparrow}=90°$, and α'' be specified at a number of values; then $|f^L_{\frac{1}{2}\frac{1}{2}\frac{\bar{1}}{2}\frac{\bar{1}}{2}}|^2$ as functions of β'' and γ'' have been observed. It was found that $\alpha''=180°$ is an optimal case, which was plotted in Fig. 6(b), where the peak is peaked at ($\beta''=90°$, $\gamma''=0°$, or 180°). It implies that e_3 and e_4 tend to stay also in the X-Z plane as shown in Fig. 5(b). Thus this state tends toward a coplanar square configuration with $\overline{OO'}$ preferably lying in the X-Y plane and with the square preferably parallel to the Z axis.

During the E-S-E oscillation of the $^1D_1^e$ and $^3P_1^e$ states, the square is not associated with a node. Thus, if the E-S-E mode is excited, an even number of nodes would appear. Hence, the excitation of the E-S-E mode may be harder than other modes. For example, the excited E-S-

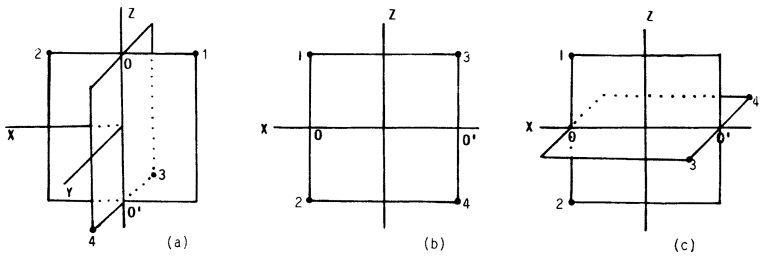

FIG. 5. Typical geometric structures and their orientations (the Z axis is lying along L). (a) A standing ETH; (b) a coplanar rectangle with the plane parallel to the Z axis; (c) a lying ETH. In these figures, 1 and 2 label the up electron, while 3 and 4 label the down electron.

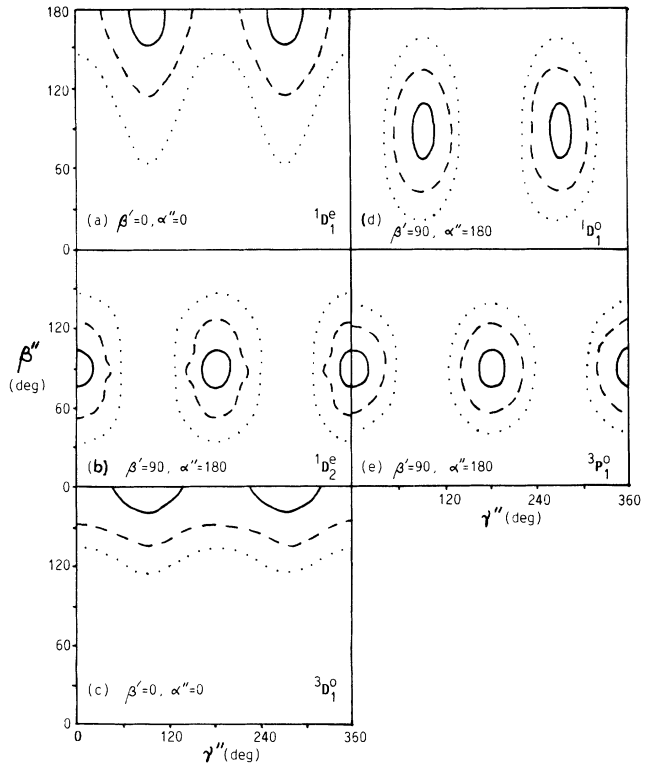

FIG. 6. $|f^L_{\frac{1}{2}\frac{1}{2}\frac{\bar{1}}{2}\frac{\bar{1}}{2}}|^2$ as functions of β'' and γ''. In each figure, $\alpha'=0°$ and $\gamma'=0°$ are assumed. β', α'', θ_{12}, and θ_{34} are given at their optimal values. β' and α'' are specified in the figure. The solid, dashed, and dotted lines give 92%, 64%, and 36% of the maximum, respectively.

E mode does appear in the $^3P_2^e$ state [refer to Fig. 6(b) of [10]] but does not appear in the $^1D_2^e$ state. We are reminded that the excitation of the E-S-E mode results in a prolongation of the ETH due to a larger amplitude of oscillation. In general, a prolonged lying ETH will cause an increase of the moment of inertia resulting in a decrease of collective rotational energy (if L is fixed) to partly compensate the increase of oscillational energy. On the contrary, a prolonged standing ETH will cause a decrease of the moment of inertia (if being confined on a sphere) resulting in an additional increase of collective rotational energy. This may be the background as to why the E-S-E mode is unlikely to be excited when the ETH is upstanding. The difference between the $^1D_2^e$ and $^1D_1^e$ states shows that geometric structures may change greatly during excitation.

V. $^3D_1^o$ STATE

The $\rho^{\frac{1}{2}\frac{1}{2}}_{\text{ori}}$ is shown in Fig. 3(c) where the distribution is peaked at $\beta'=0$. The weighted two-body densities are shown in Fig. 4(c).

Let $\alpha'=\beta'=\gamma'=0°$, and $\theta_{12}=\theta_{34}=\bar{\theta}_{\uparrow\uparrow}=100°$; then $|f^L_{\frac{1}{2}\frac{1}{2}\frac{\bar{1}}{2}\frac{\bar{1}}{2}}|^2$ with $\alpha''=0°$ is shown in Fig. 6(c), where the peak is peaked at ($\beta''=180°$, $\gamma''=90°$). This situation is just the same as the $^1D_1^e$ state; thus both states tend toward the standing ETH as predicted. However, when the $f^L_{\frac{1}{2}\frac{1}{2}\frac{\bar{1}}{2}\frac{\bar{1}}{2}}$ is observed within the same subspace as in Fig. 8(a), then the corresponding figure is given in Fig. 8(b). Where there is an INS appearing in the coplanar square configuration, it is due to the invariance under $\mathcal{P}P_{12}P_{34}$. This INS implies a stronger E-S-E oscillation; thus the $^3D_1^o$ state is higher in energy than the $^1D_1^e$ state. Besides, a stronger oscillation implies a larger amplitude; thus the ETH is more prolonged. Accordingly, the $\bar{\theta}_{\uparrow\uparrow}$ should be smaller than that of the $^1D_1^e$ state, as shown in Table I. Furthermore, Fig. 6(c) shows a smooth distribution along γ''; it implies a remarkable deformation (a standing ETH is twisted to a standing square). Accordingly, the geometric structure is not very well defined. Incidentally, if the E-S-E mode of the $^3D_1^o$ state is further excited, there would be at least three nodes involved in the oscillation resulting in very high energy. Hence, another way of

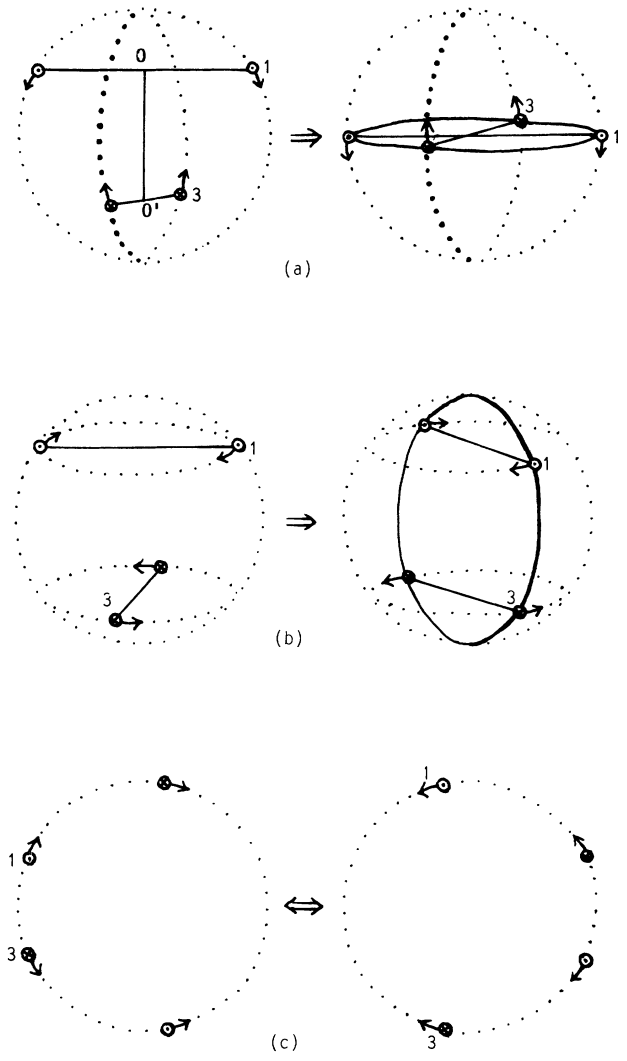

FIG. 7. Intuitive schemes of internal motion. The up and down electrons are labeled by ⊙ and ⊗, respectively. (a) The E-S-E mode, (b) the twist mode, (c) the trapezoid-rectangle-trapezoid mode. The arrows label the directions of motion of the particles.

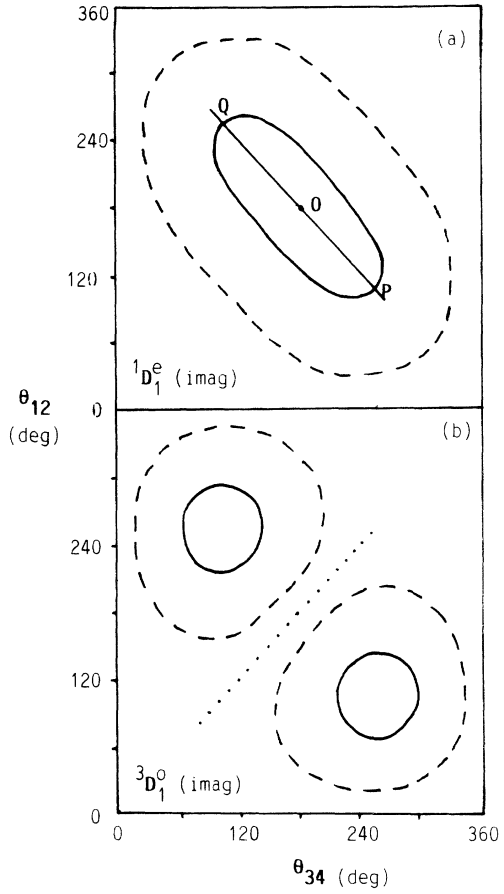

FIG. 8. $f^L_{\frac{1}{2}\frac{1}{2}\frac{\bar{1}}{2}\frac{\bar{1}}{2}}$ as functions of θ_{12} and θ_{34} to show the *E-S-E* mode. e_3 and e_4 are assumed to move in a plane normal to that of e_1 and e_2. The solid line gives $\pm 86\%$ of the maximum and the dashed line gives $\pm 32\%$. The dotted line is a nodal line.

excitation may replace the *E-S-E* excitation. In fact, the $^3D_2^o$ state (contained in the $N \geq 3$ shell) has been found to be dominated by the four-body head-on collision mode defined in [5].

VI. $^1D_1^o$ STATE

The $\rho^{\frac{1}{2}\frac{1}{2}}_{\text{ori}}$ is shown in Fig. 3(d) where the distribution is peaked at ($\beta'=90°$, $\gamma'=0°$, or 180°). The weighted two-body densities are shown in Fig. 4(d). Let $\alpha'=0°$, $\beta'=90°$, $\gamma'=0°$ [the locations of e_1 and e_2 are given as in Fig. 5(c)], and $\theta_{12}=\theta_{34}=\bar{\theta}_{\uparrow\uparrow}=102°$; then $|f^L_{\frac{1}{2}\frac{1}{2}\frac{\bar{1}}{2}\frac{\bar{1}}{2}}|^2$ with $\alpha''=180°$ (an optimal case) is shown in Fig. 6(d). Where the peak is peaked at ($\beta''=90°$, $\gamma''=90°$), it implies that the electrons, just as predicted, tend to form a lying ETH as shown in Fig. 5(c). Figure 3(d) shows a smooth distribution along γ', implying that the orientation of the ETH about the lying $\underline{OO'}$ would be quite random.

During the *E-S-E* oscillation, the intermediate square is associated with a node because it is invariant under $\mathcal{P}P_{12}P_{34}$. Hence, this state also has a strong *E-S-E* oscillation. Although the $^1D_1^o$ state and the $^3P_1^e$ ground state [10] both tend toward the lying ETH, the former is stronger both in internal oscillation and in collective rotation, resulting in much higher energy.

VII. $^3P_1^o$ STATE

The $\rho^{\frac{1}{2}\frac{1}{2}}_{\text{ori}}$ is shown in Fig. 3(e). Similar to Fig. 3(d), the distribution is also peaked at ($\beta'=90°$, $\gamma'=0°$, or 180°); when γ' changes, $\rho^{\frac{1}{2}\frac{1}{2}}_{\text{ori}}$ also varies smoothly. The weighted two-body densities are shown in Fig. 4(e), where the peak in $\tilde{\rho}_{\uparrow\downarrow}$ is broad (in fact, it is a combination of two peaks) and $\bar{\theta}_{\uparrow\downarrow}$ is particularly large.

Let $\alpha'=0°$, $\beta'=90°$, $\gamma'=0°$ and let $\theta_{12}=\theta_{34}=96°$; then $|f^L_{\frac{1}{2}\frac{1}{2}\frac{\bar{1}}{2}\frac{\bar{1}}{2}}|^2$ with $\alpha''=180°$ (an optimal case) is shown in Fig. 6(e). Where the peak is sharply peaked at ($\beta''=90°$, $\gamma''=0°$, or 180°), it implies that the electrons tend to form a coplanar rectangle [as shown in Fig. 5(b), but a little more prolonged along the Z axis]. Although there is a strong preference for $\underline{00'}$ lying the the X-Y plane, the azimuthal orientation of the rectangle about $\underline{00'}$ was found to be quite random. This fact is associated with the smooth distribution in Fig. 3(e), in accord with the variation of γ'. In this rectangle, a pair of spin-parallel electrons are placed at two adjacent vertexes, just as predicted in Sec. III. The diagonals of the rectangle give a large angular separation between an up-down pair responsible for the large $\bar{\theta}_{\uparrow\downarrow}$.

VIII. $^1P_1^o$ STATE

The $\rho^{\frac{1}{2}\frac{1}{2}}_{\text{ori}}$ of this state is isotropic; we shall discuss this point later. The weighted two-body densities are shown in Fig. 4(f), where the peak in $\tilde{\rho}_{\uparrow\downarrow}$ is broad and $\bar{\theta}_{\uparrow\downarrow}$ is particularly small. Being strongly constrained by the QM symmetry, the structure of this state is rather complicat-

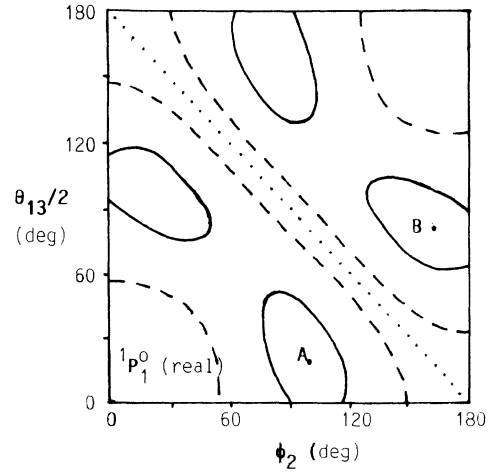

FIG. 9. $f^L_{\frac{1}{2}\frac{1}{2}\frac{\bar{1}}{2}\frac{\bar{1}}{2}}$ plotted in the X-Y plane as a function of $\theta_{13}/2$ and ϕ_2 to show the trapezoid-rectangle-trapezoid mode. Refer to the caption of Fig. 8.

TABLE II. A group of states having an ETH as their most probable shape. They are listed in different columns according to the number of nodes in the *E-S-E* mode and in different rows according to their preference of orientation. "Lying" means that OO' tends to lie in the X-Y plane normal to L. "Standing" means parallel to L.

	0	1	2
Isotropic		$^5S_1^o$	
Lying	$^3P_1^e$	$^1D_1^o$	$^3P_2^e$
Standing	$^1D_1^e$	$^3D_1^o$	

TABLE III. A group of states having a coplanar rectangle as their most probable shape; the rectangle has each pair of spin-parallel electrons staying at adjacent vertexes. The first row specifies the number of nodes in the rectangle-square-rectangle mode [6]. "Lying" means that $\overline{OO'}$ tends to lie normal to L. The internal motion of the $^1D_2^e$ state has not yet been made very clear.

	0	2	
Isotropic	$^1S_1^e$	$^1S_2^e$	
Lying	$^3P_1^o$		$^1D_2^e$

ed. Both coplanar and noncoplanar structures are found. To show the coplanar structure, let all the electrons lie in the fixed X-Y plane, so that the coordinates from e_1 to e_4 read (90°, $-\theta_{13}/2$), (90°, ϕ_2), (90°, $\theta_{13}/2$), and (90°, ϕ_4), respectively. Let $\phi_4=-\phi_2$ (this is an optimal case). Then, the real part of $f^L_{\frac{1}{2}\frac{1}{2}\frac{1}{2}\frac{1}{2}}$ (meanwhile, the imaginary part is zero) as a function of θ_{13} and ϕ_2 is plotted in Fig. 9. Where the peak A is associated with a trapezoid shown on the left side of Fig. 7(c), the antipeak B is associated with the right side. There is an INS appearing at the rectangle (as stated in Sec. III) lying between A and B. The evolution from A to B implies an energetic oscillation as shown in Fig. 7(c), which is called either the trapezoid-rectangle-trapezoid mode or the planar T2BC mode, first found in the $^3S_1^e$ state [6]. The orientation of the plane of the trapezoid is quite random, which is responsible for the isotropism of $\rho^{\frac{1}{2}\frac{1}{2}}_{\text{ori}}$. The trapezoid is the most probable shape; however, other geometric (noncoplanar) structures and other modes of motion (e.g., the 4BHC mode [5]) are also found. Further discussion is dropped to avoid tediousness.

IX. FINAL REMARKS

In Sec. III an analysis based on symmetry has been made. The outcome from this analysis is entirely supported by the results of the calculation. It implies that the main features of low-lying states, including the set of quantum numbers (L,S,π) and the morphology (i.e., the most probable shape, the most probable orientation, and the most preferred mode of motion) are decisively determined by the symmetry.

Among the 12 $N=2$ intrashell states, six of them are dominated by the ETH (prolonged or flattened) geometric structure. Where the $\overline{OO'}$ tends to be either normal or parallel to L, an intermediate case (e.g., $\overline{OO'}$ tends to make a 45° angle with L) is not found. The excitation mode is dominated by the *E-S-E* mode; hence, these states can be classified according to the number of nodes as shown in Table II. Incidentally, the twist mode is also a basic mode of the ETH structure. However, among these six states, none of them has a strong twist motion. In general, the number of nodes involved in the twist mode can be used to classify the states further.

When the ETH is no longer preferred due to the existence of nearby INS, a coplanar rectangle (including the square) would be favored. Among the 12 states, four of them possess this structure listed in Table III. In all of these states a pair of spin-parallel electrons are located at adjacent vertexes. In the $^3P_1^o$ and $^1D_2^e$ states, $\overline{OO'}$ is preferably normal to L (besides, in the $^1D_2^e$ state, the rectangle is preferably parallel to L). The excitation mode is dominated by the rectangle-square-rectangle mode [6]; hence the associated number of nodes can be used to classify the states.

When both the ETH and the coplanar rectangle are not preferred, the system may favor a noncoplanar rectangle, a coplanar trapezoid, or both. The $^3S_1^o$ state was found to possess a noncoplanar rectangle as its most probable shape with an energetic 4BHC oscillation [5]. The $^1P_1^o$ state was found to be a mixture of a coplanar trapezoid and a noncoplanar rectangle; the trapezoid-rectangle-trapezoid mode and the 4BHC mode are both found.

It was verified in [5] and [6] that all the above-mentioned basic modes, namely, the *E-S-E*, the rectangle-square-rectangle, the 4BHC, and the trapezoid-rectangle-trapezoid modes, correspond to exact periodical solutions of the classical Lagrange equations.

In higher excited states, the coexistence of difference shapes and the coupling of different modes are likely to occur. Nonetheless, the morphology and the number of nodes of different modes provide a sound physical background for the classification of states.

ACKNOWLEDGMENTS

This work is supported by the Foundation of National Natural Science of PRC, and by the Foundation of National Educational Committee of PRC.

[1] K. E. Banyard and R. J. Mobbs, J. Chem. Phys. **75**, 3433 (1981).

[2] R. J. Mobbs and K. E. Banyard, J. Chem. Phys. **78**, 6106 (1983).

[3] C. A. Nicolaides, M. Chrysos, and Y. Komninos, Phys. Rev. A **41**, 5244 (1992).

[4] K. T. Chung, X. W. Zhu, and Z. W. Wang, Phys. Rev. A **47**, 1740 (1993).

[5] C. G. Bao, Phys. Rev. A **47**, 1752 (1993).
[6] C. G. Bao and Y. W. Duan, Phys. Rev. A **49**, 818 (1994).
[7] C. G. Bao, Z. Phys. D **22**, 557 (1992).
[8] C. G. Bao, J. Phys. B **25**, 3725 (1992).
[9] M. Karplus and R. N. Porter, *Atoms and Molecules* (Benjamin, New York, 1970).
[10] C. G. Bao, J. Phys. B **26**, 4671 (1993).
[11] P. J. Li, C. G. Bao, and T. K. Lim, Few-Body Syst. **9**, 11 (1990).